Mon. Not. R. Astron. Soc. **398,** 1403–1413 (2009) doi:10.1111/j.1365-2966.2009.15190.x

X-ray spectra from magnetar candidates – III. Fitting SGR/AXP soft X-ray emission with non-relativistic Monte Carlo models

S. Zane,[1⋆] N. Rea,[2⋆] R. Turolla[1,3⋆] and L. Nobili[3⋆]

[1] *Mullard Space Science Laboratory, University College London, Holmbury St Mary, Dorking, Surrey RH5 6NT*
[2] *University of Amsterdam, Astronomical Institute 'Anton Pannekoek', Kruislaan, 403, 1098 SJ Amsterdam, the Netherlands*
[3] *Department of Physics, University of Padova, via Marzolo 8, 35131 Padova, Italy*

Accepted 2009 June 4. Received 2009 June 4; in original form 2009 March 27

ABSTRACT

Within the magnetar scenario, the 'twisted magnetosphere' model appears very promising in explaining the persistent X-ray emission from soft gamma repeaters (SGRs) and anomalous X-ray pulsars (AXPs). In the first two papers of the series, we have presented a 3D Monte Carlo code for solving radiation transport as soft, thermal photons emitted by the star surface are resonantly upscattered by the magnetospheric particles. A spectral model archive has been generated and implemented in XSPEC. Here, we report on the systematic application of our spectral model to different *XMM–Newton* and *INTEGRAL* observations of SGRs and AXPs. We find that the synthetic spectra provide a very good fit to the data for the nearly all the source (and source states) we have analysed.

Key words: radiation mechanisms: non-thermal – stars: neutron – X-rays: stars.

1 INTRODUCTION

Over the last few years, increasing observational evidence has gathered in favour of the existence of 'magnetars', i.e. neutron stars (NSs) endowed with an ultra-strong magnetic field ($B \approx 10^{14}$–10^{15} G), about ten times higher than the critical threshold at which quantum electro-dynamical (QED) effects become important ($B_{\rm crit} \sim 4.4 \times 10^{13}$ G). The family of magnetar candidates comprises two classes of sources, anomalous X-ray pulsars (AXPs) and soft γ-ray repeaters (SGRs). About fifteen objects are known, all characterized by similar properties: slow X-ray pulsations ($P \sim 2$–12 s), large spin-down rates ($\dot{P} \sim 10^{-13}$–10^{-10} s s^{-1}), a typical persistent X-ray luminosity of $\approx 10^{34}$–10^{36} erg s^{-1}, lack of bright optical companions (favouring an interpretation in terms of isolated objects), and a high level of bursting/flaring activity which can differ between the two classes (see Woods & Thompson 2006; Mereghetti 2008, for recent reviews).

Spectral data can provide key information about the physics of ultra-magnetized NSs. High-energy observations of SGRs and AXPs persistent emission now cover the ∼0.5–10 (*XMM–Newton*/*Chandra*) and ∼20–200 (*INTEGRAL*) keV bands. It is possible, although not yet proved, that different emission mechanisms are responsible for the emission in the two bands.

The low-energy ($\lesssim$10 keV) spectrum of the persistent (i.e. outside bursts) emission is often modelled in terms of a blackbody (BB, $kT \sim 0.3$–0.6 keV) plus a power law (PL) with photon index $\Gamma_s \sim 2$–4, although in some AXPs a two-blackbody model has also been applied. The X-ray persistent emission above 20 keV has a PL spectral shape ($\Gamma_h \sim 2$) which, in particular in AXPs, is markedly harder than that observed below 10 keV (see again Mereghetti 2008, and references therein). However, although these phenomenological fitting models have been systematically applied over the last decade, a convincing physical interpretation of the various spectral components is still missing.

In the magnetar framework, the twisted magnetosphere model (Duncan & Thompson 1992; Thompson & Duncan 1993; Thompson, Lyutikov & Kulkarni 2002) offers a promising physical interpretation for the X-ray emission from SGRs/AXPs. In particular, the supporting currents required to sustain the twist are substantially in excess of the Goldreich–Julian current and can produce large optical depth to resonant cyclotron scattering (RCS). Soft (thermal) photons produced at the star surface gain energy in repeated scatterings and this leads to the formation of an extended, high-energy tail, superimposed to the seed thermal component. The qualitative predictions of this model have been verified to match some spectral and timing properties of magnetar sources, as the spectral shape observed in quiescence below ∼10 keV and the long term variation observed in some sources (e.g. Mereghetti et al. 2005; Rea et al. 2005; Campana et al. 2007).

More recently, several efforts have been carried out in order to test the model quantitatively against real data using different approaches and with a varying degree of sophistication. A first attempt in this direction was presented by Lyutikov & Gavriil (2006). These authors developed a very simple, semi-analytical treatment of the RCS process by working in 1D geometry. They assumed that seed photons are emitted by the NS surface with a BB spectrum, and Thomson scattering occurs in a thin, plane parallel magnetospheric slab permeated by a static, non-relativistic, warm medium

⋆E-mail: sz@mssl.ucl.ac.uk (SZ); n.rea@uva.nl (NR); turolla@pd.infn.it (RT); nobili@pd.infn.it (LN)

at constant electron density. These models have been implemented in XSPEC by Rea et al. (2007a,b, 2008) and successfully applied to all magnetars spectra below 10 keV. The good agreement found, even within a simplified treatment, supports the idea that RCS in a sheared magnetosphere plays a central role in the formation of magnetar spectra in the (soft) X-ray range. The same RCS model has been used by Güver et al. (2007), who assumed that seed photons come from an atmosphere surrounding the star. More recently, 3D Monte Carlo calculations have been presented by Fernandez & Thompson (2007), although these spectra have never been applied to fit X-ray observations.

Motivated by this, we present here a systematic application of our 3D Monte Carlo spectral calculations (see Nobili, Turolla & Zane 2008a,b, for all details) to AXP and SGR spectral data. The paper is organized as follows. In Section 2, we briefly summarize the basic features of the model. The data sample and spectral results are presented in Section 3. Discussion and conclusions follow in Sections 4 and 5, respectively.

2 THE MODEL

As discussed in detail in Nobili et al. (2008a,b), we have recently developed a 3D treatment of RCS, aimed at a detailed investigation of the spectral, timing and polarization properties of magnetars (see also Pavan et al. 2009). Our Monte Carlo code, which is completely general and can handle different magnetic field topologies and distributions of seed photons, has been used to produce an archive of spectral models that have been subsequently implemented in XSPEC. Such models rely on a number of choices for the assumed configuration, that are discussed in detail in Nobili et al. (2008a) and briefly summarized in this section.

First, the XSPEC archive models have been computed by assuming that the star surface emits as a BB at an uniform temperature, kT, and that the surface radiation is isotropic and unpolarized. The magnetic field topology is assumed to be a twisted, force free dipole and is uniquely characterized by the value of the twist angle, $\Delta\phi$ (see Thompson et al. 2002). No attempt is made to fit the value of the polar field strength, that has been fixed at 10^{14} G. Our model is based on a simplified treatment of the charge carriers velocity distribution which accounts for the particle collective motion, in addition to the thermal one. Pair production has been neglected. Magnetospheric electrons stream freely along the field lines (the motion across the field lines is quantized). The electron velocity distribution parallel to the field is taken to be a 1D relativistic Maxwellian at temperature $T_{\rm e}$, superimposed to a bulk motion with velocity $\beta_{\rm bulk}$ (in units of the light velocity c). Additionally, in order to minimize the number of free parameters, the models in the archive were computed assuming that the electron temperature is related to $\beta_{\rm bulk}$ (see Nobili et al. 2008a, for all details). Scattering in a magnetized medium was treated by considering only the resonant part of the magnetic Thomson cross-section and neglecting electron recoil along the field direction. For the sake of conciseness, in the following this approximation will be referred to as the (resonant) Thomson limit. On the other hand, the code is completely general, and includes the relativistic QED resonant cross-section, which is required in the modelling of the hard ($\sim$20–200 keV) spectral tails observed in the magnetar candidates (see Nobili et al. 2008b; Pavan et al. 2009). Electron recoil in the direction parallel to the field starts to be important when the photon energy in the electron rest frame becomes comparable to the electron rest energy. If γ is the mean electron Lorentz factor, this occurs at typical energies $\sim m_{\rm e}c^2/\gamma$. Assuming mildly relativistic particles, the previous limit implies that conservative scattering should provide good accuracy up to photon energies of some tens of keV. This, together with the fact that resonant scattering occurs in regions where $B \ll B_{\rm crit}$, makes the use of the (much simpler) non-relativistic (Thomson) magnetic cross-section adequate. The final XSPEC *atable* spectral model (22 MB in size, named *ntznoang.mod*, hereafter NTZ) has been created by using the routine *wftbmd*, available on-line.[1] In summary, it depends on four free parameters ($\beta_{\rm bulk}, \Delta\phi, \log kT$ plus a normalization constant), which can be simultaneously varied during the spectral fitting following the standard χ^2 minimization technique. In the NTZ models, the photon number is conserved and the monochromatic number flux which reaches infinity is the same as that of the seed BB spectrum.[2] This implies that the normalization constant (norm) divided by kT^3 is proportional to the emitting area on the star surface (see Section 4.2). It is important to note that the NTZ model has the same number of free parameters as the canonical BB plus PL empirical model or the 1D RCS model recently discussed in Rea et al. (2008), and hence has the same statistical significance. In the following sections, we present its systematic application to the soft (0.5–10 keV) X-ray spectra of magnetar candidates.

3 APPLICATION TO MAGNETAR'S SOFT X-RAY SPECTRA

We applied the NTZ model to a large sample of AXPs and SGRs, using *XMM–Newton* and *INTEGRAL* data. The sample of data sets basically coincides with that used in Rea et al. (2008), and we refer to that paper for more details and for a discussion on the data analysis. However, unlike Rea et al. (2008), we did not consider here the transient magnetars XTE J1810−197 and CXOU J1647−4552, the analysis of which will be reported in a separate paper devoted to a detailed investigation of their outburst evolution over a period of several years. On the other hand, we included the recent *XMM–Newton* observations of CXOU J0100−7211 and SGR 1627−41, that were not available at the time of the previous investigation (see Esposito et al. 2009; Tiengo, Esposito & Mereghetti 2008, for further details on these observations).

All fits have been performed using XSPEC version 11.3 and 12.0, for a consistency check. A 2 per cent systematic error was added to the data to partially account for uncertainties in instrumental calibrations. Only in the case of CXOU J0100−7211, which has a very low absorption, the fit has been performed in the 0.5–10 keV energy range. For the other sources, that are highly absorbed, the 0.5–1 keV energy range (0.5–2 keV energy range in the case of SGR 1627-41) was excluded from our spectral fitting.[3] We then checked that, for all our targets, the values of $N_{\rm H}$ derived fitting the 1–10 keV EPIC-pn spectra, are consistent (within 1σ) with those

[1] see http://heasarc.gsfc.nasa.gov/docs/heasarc/ofwg/docs/general/modelfiles_memo/modelfiles_memo.html.

[2] Photon number is not necessary conserved when Landau-Raman scattering is accounted for (photon spawning; Nobili et al. 2008b). Present models have been obtained under the assumption of conservative magnetic scattering, so photon number conservation is ensured. Also, spectra in the model archive have been computed averaging over all viewing directions, i.e. photons are collected over the entire observer's sky. When one particular line of sight (LOS) is chosen, the photons reaching the observer are clearly less than those emitted by the surface.

[3] The emission in this energy range is in fact mostly affected by interstellar absorption. Moreover, this is the band where most of the calibration issues lay (Haberl et al. 2004).

Table 1. Spectral Parameters of 1RXS J1708−4009, 1E 1841−045, SGR 1900+14, CXOU J0100−7211 and SGR 1627−41 obtained by fitting the *XMM–Newton* data with an NTZ model. The fit has been restricted to the 1–10 keV range, with the exception of CXOU J0100−7211 and SGR 1627−41 for which we used the 0.1–10 and 2–10 keV band, respectively. Errors are at 1σ confidence level, reported fluxes are absorbed and in units of erg s^{-1} cm^{-2}. $N_{\rm H}$ is in units of 10^{22} cm^{-2}, and we assumed solar abundances from Lodders (2003). See also Figs 1 and 2, and Section 3 for details.

Parameters	1RXS J1708–4009*	1E 1841–045	SGR 1900+14	CXOU J0100-7211	SGR 1627-41
N_H	1.45 ± 0.08	2.5 ± 0.1	3.74 ± 0.15	<0.05	12 ± 1
kT (keV)	0.47 ± 0.09	0.50 ± 0.06	0.45 ± 0.04	0.35 ± 0.02	0.64 ± 0.11
$\beta_{\rm bulk}$	0.34 ± 0.04	0.43 ± 0.05	0.46 ± 0.05	0.18 ± 0.03	0.7 ± 0.1
$\Delta\phi$	0.49 ± 0.15	0.47 ± 0.04	0.45 ± 0.03	1.7 ± 0.8	1.3 ± 0.4
NTZ norm	0.35 ± 0.04	0.20 ± 0.02	0.08 ± 0.02	0.004 ± 0.001	0.005 ± 0.001
Flux (1–10 keV)	$(2.6 \pm 0.2) \times 10^{-11}$	$(2.1 \pm 0.2) \times 10^{-11}$	$(3.9 \pm 0.3) \times 10^{-12}$	$(3.3 \pm 0.2) \times 10^{-13}$	$(3.3 \pm 0.2) \times 10^{-13}$
χ^2_ν (d.o.f.)	0.97 (197)	1.04 (152)	0.99 (135)	1.21 (101)	1.16 (81)

*Source slightly variable in flux and spectrum, see text for details.

obtained using the 0.5–10 keV range relative to the same data set. We used the more updated solar abundances by Lodders (2003), instead of the older ones from Anders & Grevesse (1989). As a consequence, the value of the absorption is, on average, slightly higher than that reported in the literature for the same model. This does not affect the other spectral parameters.

Table 1 and Figs 1 and 2 report our results in the 1–10 keV range for those sources that do not show a substantial spectral variation, in which cases only one data set (the longest available) has been considered. Also, in Tables 2 and 3 and Fig. 3, we show the fits for sources that do exhibit spectral variation, in which cases we considered a set of two or three observations for each source, corresponding to different spectral states. At variance with Rea et al. (2008), in these cases the different data sets have been fitted by imposing that the absorption, $N_{\rm H}$, is the same. As can be seen from the tables, in most of the cases, we found that a NTZ model alone successfully reproduces the soft X-ray part of the spectrum up to 10 keV, without the need of further components (see Section 4 for a discussion). With reference to the sample considered in Rea et al. (2008), the only two sources for which we do not find a satisfactory fit are 1E 2259+586 and 4U 0142+614, which are discussed separately below.

There are a few AXPs and SGRs in our sample (namely 1RXS J1708−4009, 1E 1841−045, 4U 0142+614, 1E 2259+586, SGR 1900+14 and SGR 1806−20) that are known to have a conspicuous emission in the hard X-ray band. For these objects, we repeated our modelling including also their *INTEGRAL* spectra in order to investigate whether our model can reproduce part of the emission when considering the whole spectral energy distribution (SED).[4] A further PL has been introduced in order to account for the non-thermal hard X-ray component, although at a purely phenomenological level. A free constant was multiplied when using both *XMM–Newton* and *INTEGRAL* data to account for intercalibration uncertainties (the values of the constant was always differing by less than 10 per cent with respect to *XMM–Newton* which was set to unity). Results are reported in Table 4 and Fig. 4. We find that, again with the exception of 1E 2259+586 and 4U 0142+614, in all other cases, a NTZ+PL spectral decomposition successfully models the 1–200 keV emission. However, the fit converges with a hard X-ray component that gives a substantial contribution when extrapolated to the soft X-ray band and, consequently, the best-fitting parameters of the NTZ model are substantially different from those we found fitting the 1–10 keV emission only.

As the tables show, in some cases the fit converges with a value of $\Delta\phi$ which is too close to the upper bound of our model archive ($\Delta\phi = 2$), making impossible to compute the whole (closed) 1σ contour level. Indeed, in the case of the combined *XMM–Newton* and *INTEGRAL* fits of 1E 1841−045 and SGR 1900+14, the parameters of the NTZ model becomes less constrained than when fitting the *XMM–Newton* data alone, and we could only set an upper limit on $\Delta\phi$ (see Table 4). Although we do not regard this as a particular problem, we should note the caveat that in some fits, the value of the twist angle appears to be less constrained than those of the other model parameters.

4 DISCUSSION

In this paper, we have applied a 3D Monte Carlo model of resonant scattering to the phase averaged spectra of an extensive set of magnetar sources. The sample is the same as in Rea et al. (2008), with the exception of the two transient magnetars XTE J1810−197 and CXOU J1647−4552, and with the inclusion of recent *XMM–Newton* observations of CXOU J0100−7211 and SGR 1627−41. The discussion of our findings is organized as follows. In Section 4.1, we first concentrate on the results emerging from the fit of the *XMM–Newton* data only, that is on the energy band below 10 keV. We report the discussion of our spectral results, a comparison with the analogous findings from the 1D RCS fits of Rea et al. (2008), and we discuss the cases of 1E 2259+586 and 4U 0142+614, that is the only two sources for which a fit with the NTZ model is unsatisfactory. A search for correlations among the sources and the model parameters, in the same energy band, is reported in Section 4.2. In Section 4.3, we then discuss the NTZ model in the contest of the interpretation of the whole SED up to ∼200 keV, basing this time on both *XMM–Newton* and *INTEGRAL* data. The main limitations and caveats are then summarized in Section 4.4.

4.1 The soft X-ray spectra: fits of the *XMM–Newton* data

Our results on the fits of the *XMM–Newton* data are reported in Table 1 and Figs 1 and 2 for sources without a significant spectral

[4] In the case of SGR 1806−20, there are no observations taken at similar epochs in the hard and soft X-ray bands. For this reason, and because of the high variability of this source, no attempt has been made to fit its broad-band distribution either here or in Rea et al. (2008).

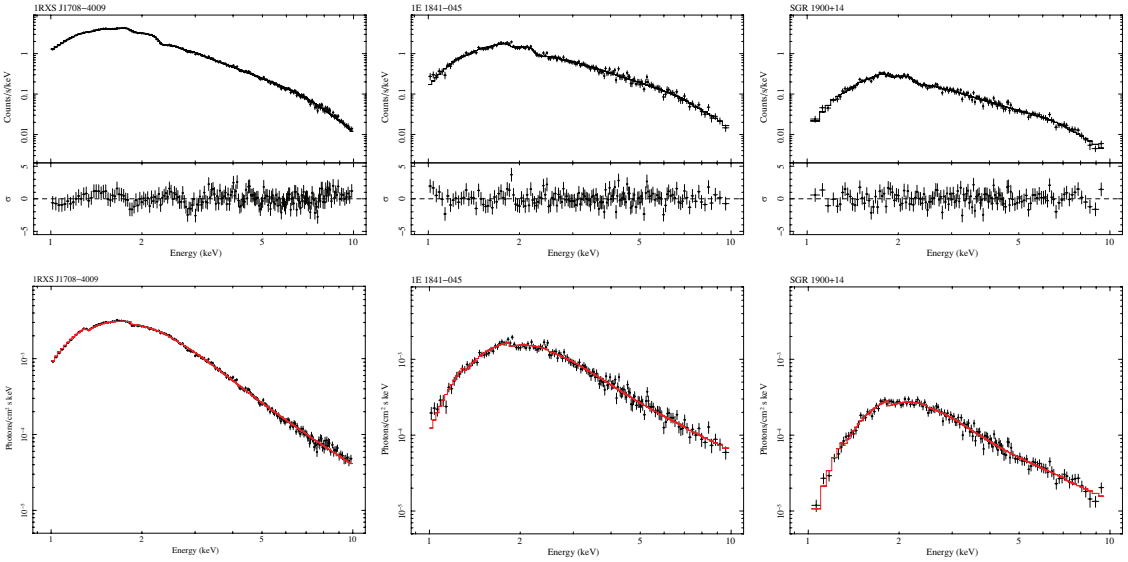

Figure 1. 1RXS J1708−4009, 1E 1841−045 and SGR 1900+14: first row shows the spectra in count s^{-1} keV^{-1} while in the second row we report the photon density plots of the modelling with the NTZ model. Only *XMM–Newton* data have been used, and the fitting has been restricted to the 1–10 keV range. See Table 1 and Section 3 for details.

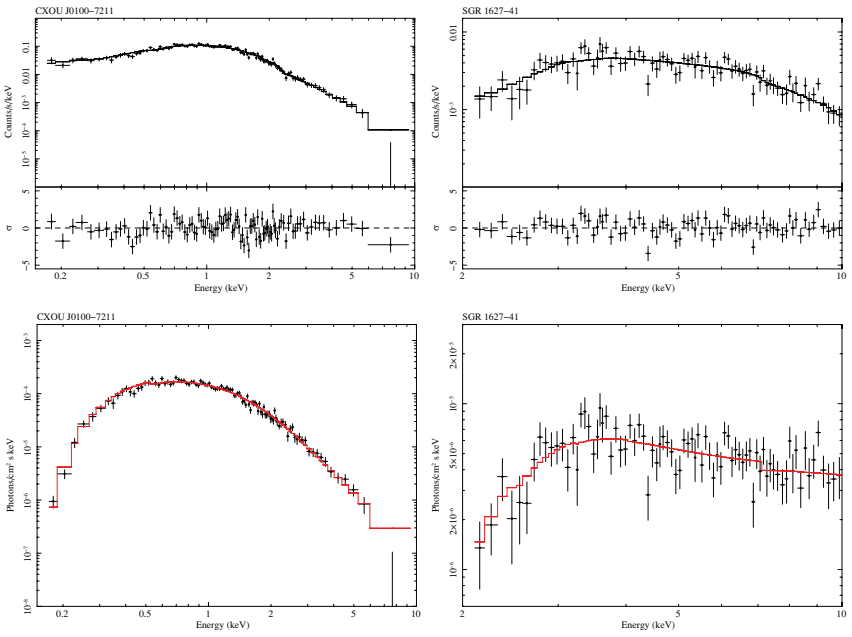

Figure 2. Same as in Fig. 1 for CXOU J0100−7211 and SGR 1627−41. See Table 1 for details.

variation, and in Tables 2 and 3 and Fig. 3 for sources that do exhibit spectral variation. When we restrict to the 1–10 keV band, we found that the NTZ model successfully reproduces the soft X-ray part of the spectrum of most of the sources (apart from 1E 2259+586 and 4U 0142+614), without the need of additional components. This represents a substantial improvement with respect to previous attempts to model magnetars quiescent emission in the same energy band with a simpler 1D RCS model (Rea et al. 2008), where it was found that in a few cases a PL component was required, in addition to the RCS one, to provide an acceptable fit to the data below 10 keV. In particular, this was the case of a few AXPs (including e.g. 1RXS J1708−4009 and 1E 1841−045) and of SGR 1806−20, all them detected also above $\gtrsim$20 keV. In such cases, we found that the 1D RCS component reproduces the spectrum only up to 5–8 keV. In order to match the data at the highest *XMM–Newton* energies, the contribution of a PL must be included. On the other hand, the slope of this additional PL is the same of that describing the *INTEGRAL* spectrum in the ∼20–200 keV band. It is very possible that the mechanism responsible for the hard X-ray emission provides a non-negligible contribution in the soft X-ray range. However, our finding is that the resonant Compton scattering model by Nobili et al. (2008a) correctly describes the data in the whole *XMM–Newton* energy range, that is up to 10 keV, for all the sources (and source states) reported in Tables 1–3. The application of the NTZ model to the $\gtrsim$20 keV emission from magnetars is discussed later on. It is worth noting that the NTZ model has two free parameters less than

Table 2. Spectral parameters of 1E 1547.0−5408 and 1E 1048−5937 in different emission states, obtained by fitting the *XMM–Newton* observations with an NTZ model. The fit has been restricted to the 1–10 keV range. Errors are at 1σ confidence level, reported fluxes are absorbed and in units of erg s^{-1} cm^{-2}. $N_{\rm H}$ is in units of 10^{22} cm^{-2}, and we assumed solar abundances from Lodders (2003). See also Fig. 3.

	1E 1547.0-5408		1E 1048-5937		
Parameters	2006	2007	2003	2005	2007
$N_{\rm H}$	4.6 ± 0.13			0.66 ± 0.02	
kT (keV)	0.38 ± 0.01	0.56 ± 0.01	0.60 ± 0.06	0.56 ± 0.08	0.69 ± 0.02
$\beta_{\rm bulk}$	0.15 ± 0.05	0.4 ± 0.1	0.14 ± 0.03	0.16 ± 0.07	0.13 ± 0.04
$\Delta\phi$	1.14 ± 0.08	0.4 ± 0.1	1.9 ± 0.2	2.0 ± 0.2	1.9 ± 0.1
NTZ norm	0.02 ± 0.01	0.082 ± 0.005	0.10 ± 0.03	0.07 ± 0.01	0.21 ± 0.01
Flux (1–10 keV)	$(3.3 \pm 0.2) \times 10^{-13}$	$(3.0 \pm 0.2) \times 10^{-12}$	$(1.1 \pm 0.2) \times 10^{-11}$	$(8.3 \pm 0.4) \times 10^{-12}$	$(3.0 \pm 0.2) \times 10^{-11}$
χ^2_ν (d.o.f.)	1.11 (164)			1.22 (515)	

Table 3. Spectral Parameters of SGR 1806−20 in different emission states, obtained by fitting the *XMM–Newton* observations with an NTZ model. The three data sets have been taken before and after the giant flare of 2004 December 27 (Hurley et al. 2005; Palmer et al. 2005), with the intermediate observation taken about two months before the event. The fit has been restricted to the 1–10 keV range. Errors are at 1σ confidence level, reported fluxes are absorbed and in units of erg s^{-1} cm^{-2}. $N_{\rm H}$ is in units of 10^{22} cm^{-2} and we assumed solar abundances from Lodders (2003). See also Fig. 3.

	SGR 1806−20		
Parameters	2003	2004	2005
$N_{\rm H}$		$9.1 \pm 0.5\}$	
kT (keV)	0.69 ± 0.10	0.79 ± 0.10	0.74 ± 0.15
$\beta_{\rm bulk}$	0.48 ± 0.05	0.52 ± 0.05	0.51 ± 0.05
$\Delta\phi$	1.8 ± 0.8	1.7 ± 0.7	1.0 ± 0.9
NTZ norm	0.11 ± 0.05	0.23 ± 0.05	0.12 ± 0.08
Flux (1–10 keV)	$(1.2 \pm 0.1) \times 10^{-11}$	$(2.6 \pm 0.2) \times 10^{-11}$	$(1.3 \pm 0.2) \times 10^{-11}$
χ^2_ν (d.o.f.)		0.98 (288)	

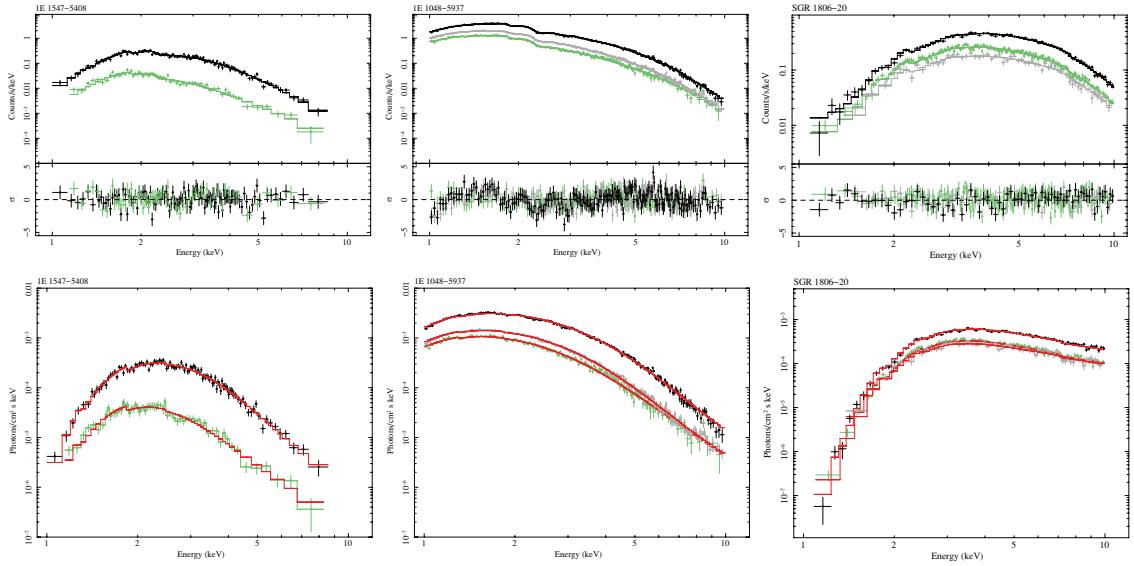

Figure 3. Same as in Fig. 1 for the AXPs 1E 1547.0−5408, 1E 1048−5937 and for SGR 1806−20. See Tables 2 and 3 for details.

the 1D RCS+PL model used in Rea et al. (2008). Hence, besides self-consistency, it is also more robust on a statistical ground.

In all the cases, we found that $N_{\rm H}$, as derived from the NTZ model, is lower than (or consistent with) that inferred from the BB+PL fit, and consistent with what derived from fitting the single X-ray edges (Durant & van Kerkwijk 2006). The same was also true for the fits with the 1D RCS model presented in Rea et al. (2008). This is not surprising, since the PL usually fitted to magnetar spectra in the

Table 4. Spectral Parameters of 1RXS J1708−4009, 1E 1841−045 and SGR 1900+14 obtained by fitting the ∼1–200 keV *XMM–Newton* and *INTEGRAL* data with an NTZ+PL model. A constant function has been included to the modelling to take into account for intercalibration uncertainties (always <10 per cent). Errors are at 1σ confidence level, reported fluxes are absorbed and in units of erg s^{-1} cm^{-2}. $N_{\rm H}$ is in units of 10^{22} cm^{-2} and we assumed solar abundances from Lodders (2003). See also Fig. 4 and Section 3 for details.

Parameters	1RXS J1708–4009* NTZ+PL	1E 1841–045 NTZ+PL	SGR 1900+14 NTZ+PL
$N_{\rm H}$	1.67 ± 0.03	2.5 ± 0.1	3.9 ± 0.2
kT (keV)	0.39 ± 0.04	0.50 ± 0.06	0.43 ± 0.06
$\beta_{\rm bulk}$	0.20 ± 0.05	0.17 ± 0.06	0.10 ± 0.08
$\Delta\phi$	1.90 ± 0.04	>0.72	>0.38
NTZ norm	0.42 ± 0.04	0.28 ± 0.03	0.06 ± 0.01
Γ	0.96 ± 0.07	1.46 ± 0.08	1.87 ± 0.09
PL norm	$(2.4 \pm 0.1) \times 10^{-4}$	$(2.1 \pm 0.1) \times 10^{-3}$	$(1.1 \pm 0.1) \times 10^{-3}$
Flux (1–10 keV)	$(2.6 \pm 0.2) \times 10^{-11}$	$(2.1 \pm 0.2) \times 10^{-11}$	$(3.9 \pm 0.3) \times 10^{-12}$
Flux (1–200 keV)	$(1.1 \pm 0.2) \times 10^{-10}$	$(1.1 \pm 0.2) \times 10^{-10}$	$(1.5 \pm 0.3) \times 10^{-11}$
χ^2_ν (d.o.f.)	1.05 (205)	1.12 (158)	1.02 (140)

*Source slightly variable in flux and spectrum, see text for details.

soft X-ray range is well known to overestimate the column density.[5] The surface temperature we derived fitting the NTZ model is slightly higher than the corresponding 1D RCS temperature and consistent with the BB temperature in the BB+PL model. On the other hand, a quantitative comparison between the values of $\beta_{\rm bulk}$ and $\Delta\phi$ (that is the parameters that describe the magnetospheric currents in the NTZ model) and the corresponding parameters of the 1D RCS model (β_T and $\tau_{\rm res}$) is more difficult, due to the different assumptions about the currents velocity distribution and the magnetic field topology. The 1D RCS assumes a plane parallel slab (i.e. photons can only propagate along the slab normal either towards or away from the star). Moreover, magnetospheric charges are assumed to have a top-hat velocity distribution centred at zero and extending up to a given temperature, $\pm kT_{\rm e}$. To some extent, this scenario mimics a thermal, 1D, motion (in which case $kT_{\rm e}$ can be assimilated to a mean e^- energy, that is to the temperature of the 1D electron plasma). Since the e^- velocity distribution averages zero, no bulk motion is accounted for: if we only consider the frequency shift due to the e^- motion then a photon has the same probability of undergoing up or down scattering. Photon boosting by particle thermal motion in Thomson limit may still occur because the spatial variation of the magnetic field is taken into account. For a photon propagating from high to low magnetic fields, multiple RCS will, on average, up-scatter the transmitted radiation, giving rise to the formation of a hard tail. Since, at variance with the 1D RCS model, our code accounts for both bulk and thermal motion, one may expect to find a value of $\beta_{\rm bulk}$ systematically lower than the value of the velocity parameter β_T in the 1D RCS fits. However, we find that this is not always the case and the relation between the values of $\beta_{\rm bulk}$ and β_T appears to be more complex. The NTZ model does not explicitly contain the optical depth as a parameter. However, $\Delta\phi$ and $\beta_{\rm bulk}$ can be related to the (average) scattering depth, as discussed in Rea et al. (2008). In particular, the value of $\tau_{\rm ave}$ can be read off from their fig. 10, simply by dividing the value of the depth corresponding to a given $\Delta\phi$ by $\beta_{\rm bulk}$. The values of $\tau_{\rm ave}$ we derive (∼0.1–1, as expected since the average number of scatterings for a typical photon is of this order) are systematically lower than those obtained for the 1D RCS $\tau_{\rm res}$. This means that the 1D RCS model is intrinsically less efficient in up-scattering the seed photons. Its spectrum is, in fact, softer and it requires a larger depth (and hence a larger number of scatterings). Moreover, the hardest sources require an additional PL to match the observed *XMM–Newton* spectra. When observations of the same source at different epochs are available, it is of interest to check if the best-fitting values of the model parameters change, since this can reveal how the physical properties of the surface/magnetosphere evolve in time. In the case of 1E 1048−5937, all the parameters are compatible with being constant within the errors, with the only exception of the normalization which appears to increase following the flux rise. The same holds for SGR 1806−20, where there may also be an indication for a decrease in the twist angle after the giant flare of 2004 December 27. Errors are however quite large and prevent any firm conclusion at this stage. The time behaviour of 1E 1547.0−5408 is puzzling, since $\beta_{\rm bulk}$ increases while $\Delta\phi$ decreases as the flux, and the model normalization, increases. In this source, there is also a quite robust evidence that the surface temperature increased with the flux.

As we mentioned before, in the case of 1E 2259+586 and 4U 0142+614 we were unable to find a satisfactory fit with the NTZ model. We noted that, below 10 keV, these two sources are characterized by a rather soft spectrum: in the canonical BB+PL decomposition the PL index is ∼4 instead of ∼2–3 as in the other magnetars. At the same time, the PL tail starts very close to the energy at which the BB peaks. Such a spectral shape appears difficult to explain in terms of upscattering of soft photon, whatever the nature of the Comptonization process might be. In fact, a PL component that starts close to the BB peak is a signature of a full-fledged Comptonization in which case, however, it is expected to be quite flat. Conversely, a steep PL tail is a typical of weak Comptonization, and departures from the BB spectrum occur at energies beyond the peak. One possible explanation is that the BB peak *appears* to be less prominent to the observer because the region that emits the soft seed photons is not coming completely into view. In Nobili et al. (2008a), we considered the effects of a non-homogeneous surface

[5] This is because the fitting procedure tends to increase absorption (i.e. $N_{\rm H}$) to counter the steep rise of the PL at low energies, which eventually diverges as $E \to 0$.

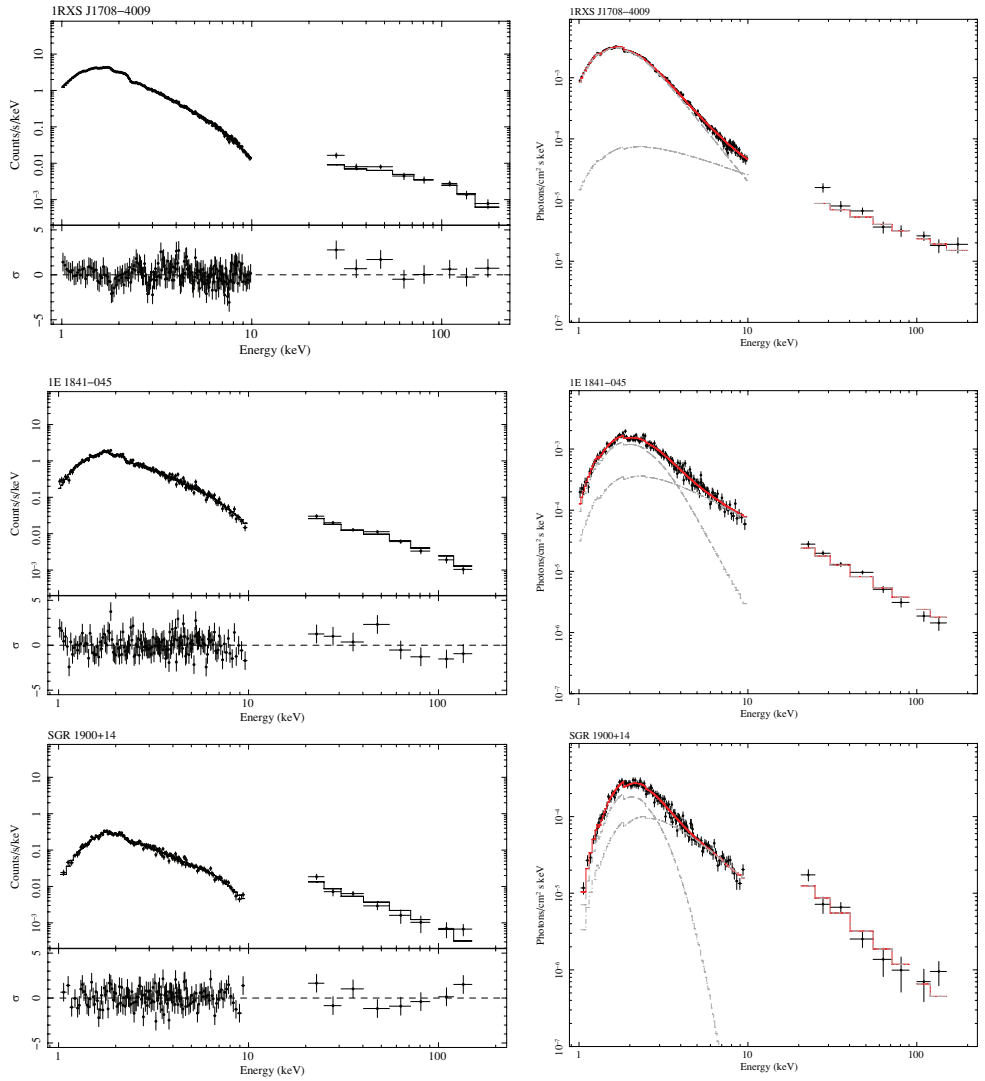

Figure 4. 1RXS J1708−4009, 1E 1841−045 and SGR 1900+14: left-hand column shows the spectra in count s^{-1} keV^{-1} while in the right-hand column we report the photon density plots of the modelling with the NTZ+PL model. Both *XMM–Newton* and *INTEGRAL* data have been used in the fitting. See Table 4 and Section 3 for details.

temperature distribution, by examining the case in which photons are emitted by a single surface patch. In Fig. 5, we show the results of our simulations in the case in which the emitting region is confined to an equatorial strip (left-hand panel) or to a polar cap (right-hand panel). The subdivision of the star surface, that of the sky, the energy range and bin width are the same as that used in Nobili et al. (2008a; see fig. 7 in that paper). The different curves show the emerging spectrum, as viewed by an observer whose LOS makes an angle Θ_s with the spin axis and for different values of the observing longitude, $\Phi_s = 20^\circ, 140^\circ$ and 220°. These three values correspond to having the emitting surface patch in full view (seen nearly face on), partially in view and almost screened by the star. As it can be seen, when the emitting patch is in full view the observed spectrum consists of a well visible thermal component and an extended PL-like tail. On the other hand, if the emitting region is not directly visible, no contribution from the primary BB photons is present: the spectrum, which is made up only by those photons which after scattering propagate 'backwards', has a depressed thermal peak and a much more distinct non-thermal shape. In particular, in the examples of Fig. 5, the scattering efficiency is not very high and curves corresponding to $\Phi_s = 220^\circ$ have a steep PL tail with photon index ∼4, as observed in 1E 2259+586 and 4U 0142+614. Although a quantitative fit of the spectra of these two sources including different thermal maps in the code would be unfeasible (because it would introduce too many degrees of freedom), it is tempting to speculate that the peculiar spectrum of 1E 2259+586 and 4U 0142+614 is due to a strong inhomogeneity in the surface temperature distribution, with the hotter region almost antipodal with respect to the observer. This is also compatible with the fact that these two sources have a rather low pulsed fraction with respect to other magnetars. On the other hand, the double peaked pulse profile of 1E 2259+586 is difficult to explain in this picture. Another possibility is that the phase average spectrum appears to be quite soft because it reflects the contribution of different components. As discussed by Woods et al. (2004) and Rea et al. (2007c), both these sources exhibit a strong spectral variation with spin phase. In the case of 4U 0142+614, the spectrum switches from being very hard to very soft within a 0.1-wide phase interval and *XMM–Newton* data reveal a discontinuity, between 2 and 3 keV, which can be interpreted as a curved component and is most apparent within phase

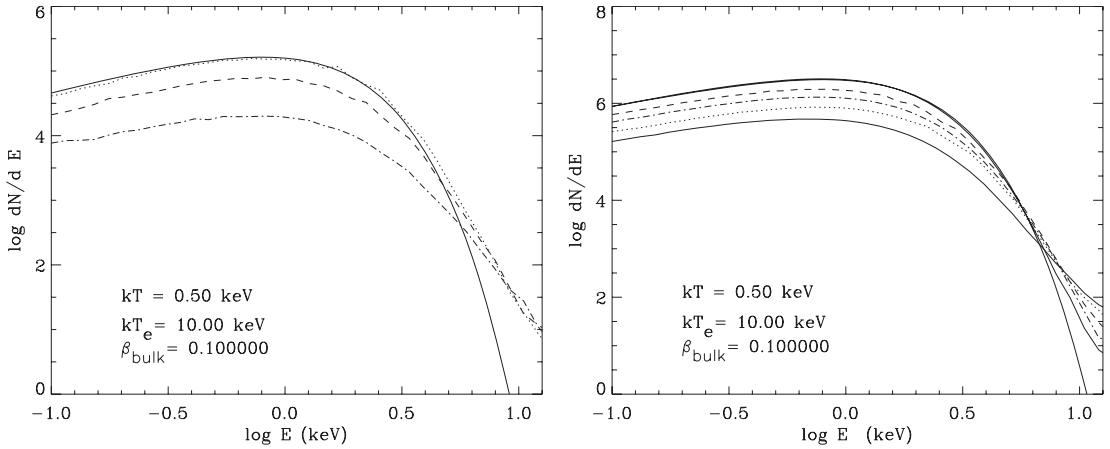

Figure 5. Spectrum from a single emitting zone on the star surface, computed as in Nobili et al. (2008a, see fig.7 in that paper and text for details). Left-hand panel: the emitting area is the equatorial strip $0 \leq \cos\Theta \leq 0.25$, $0 \leq \Phi \leq \pi/2$. The LOS is at $\Theta_s = 90^\circ$ and $\Phi_s = 20^\circ$ (dotted line), $\Phi_s = 140^\circ$ (dashed line) and $\Phi_s = 220^\circ$ (dash–dotted line). The solid line represents the seed BB. Right-hand panel: the emitting area is the polar cap $0.75 \leq \cos\Theta \leq 1, 0 \leq \Phi \leq 2\pi$. The LOS is at $\Theta_s = 19.^\circ5$ (dash-triple dotted line), $\Theta_s = 63.^\circ5$ (dashed line), $\Theta_s = 90^\circ$ (dash–dotted line), $\Theta_s = 123.^\circ5$ (dotted line) and $\Theta_s = 160.^\circ5$ (lower solid line). The upper solid line is the seed BB spectrum.

interval 0.7–0.9 (Den Hartog et al. 2008a). In order to assess this scenario, a more detailed investigation of the pulse resolved spectra is necessary; this requires the introduction of the viewing geometry in our fits and will be presented in a forthcoming paper.

4.2 Correlations

We run a number of Spearman's rank correlation tests, in order to look for possible links among the observed properties of the sources in our sample and the model parameters. In particular, we checked for correlations between the 1–10 keV luminosity, $L_{1-10\,\mathrm{keV}}$ or the spin-down value of the magnetic field, B, and each of the NTZ parameters, kT, β_{bulk} and $\Delta\phi$. The values of the parameters are those obtained from the fit of the *XMM–Newton* data only (Tables 1–3). The source distances and the values of B have been taken from the compilation in Rea et al. (2008). The only significant correlations which emerged are those between β_{bulk} and $L_{1-10\,\mathrm{keV}}$ and β_{bulk} and B. Both show a deviation from the null hypothesis probability of $\sim$93 per cent. Although the significance level is lower, 81 per cent, a correlation between kT and $L_{1-10\,\mathrm{keV}}$ seems also to be present. The correlation between $L_{1-10\,\mathrm{keV}}$ and β_{bulk}, which is direct, can be explained taking into account that an increase of β_{bulk} results in a larger energy gain of the photons per scattering and hence in a hardening of the spectrum, which translates into a higher luminosity. A similar argument applies to the $L_{1-10\,\mathrm{keV}}$–kT correlation, which is again direct. An increase of the surface temperature implies an increase of the flux of primary photons and again of the observed luminosity. The β_{bulk}–B correlation mirrors that between β_T and B reported in Rea et al. (2008), and, as discussed there, is not of immediate interpretation.

As discussed in Nobili et al. (2008a), the modulation of the X-ray flux may be due to the anisotropy of the magnetospheric charge density (which is lower along the poles), to a patchy surface temperature distribution or to a combination of both effects. As mentioned in Section 2, in the NTZ models, the normalization constant (norm) divided by kT^3 is proportional to the emitting area on the star surface. To check if the observed modulation is related (also) to the presence of a hotter region on the surface, we looked for a correlation between the pulsed fraction and the ratio norm $\times D^2/kT^3$, where D is the source distance. The pulsed fraction is defined as

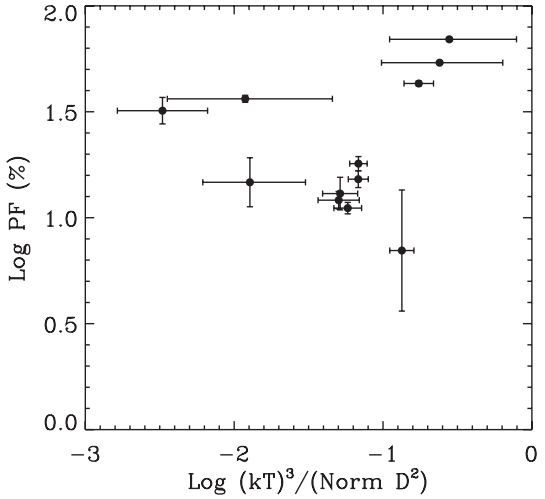

Figure 6. The pulsed fraction versus a measure of the surface emitting area for the AXPs in our sample; see text for details. Five more recent observations of 1E 1547.0−5408 have been also included in this plot (Bernardini et al., in preparation).

the semi-amplitude of the sinusoidal function that best fits the light curve, in the same energy range. We run the test on the entire sample of sources, excluding the first observation of 1E 1547.0−5408, for which only an upper limit of the pulsed fraction is available. No significant correlation was found. However, when the sample is restricted to AXPs only, a negative correlation (i.e. the pulsed fraction increases when the area decreases) emerges at the 91 per cent confidence level. To verify this, we run again the test including the data from a set of five more recent observations of 1E 1547.0−5408 (Bernardini et al., in preparation) and found that the correlation is still present, although the significance level slightly decreases to 74 per cent (see Fig. 6). Taken face value, this results points towards a localized emitting area in AXPs while the surface temperature would be more uniform in SGRs, where the modulation is produced mainly by scatterings in the magnetosphere. We note that the presence of a (time varying) hot spot has been reported in some

transient AXPs, but the existence of a general pattern as the one discussed above needs a larger sample to be confirmed.

Finally, we checked whether there is a correlation between $\Delta\phi$ and $\beta_{\rm bulk}$. The motivation for this is that both parameters are responsible for the formation of the high-energy tail. This may introduce a redundancy in the model parameters: in principle, the fit might be not unique, since quite similar spectra may be obtained with different combinations of $\Delta\phi$ and $\beta_{\rm bulk}$ (e.g. low $\beta_{\rm bulk}$ and large $\Delta\phi$ or the opposite). We did not find any significant correlation between these two quantities.

4.3 The broad-band spectrum in the 1–100 keV range

As discussed in Section 3, a spectral decomposition of the kind NTZ+PL successfully reproduces the whole spectrum of 1RXS J1708−4009, 1E 1841−045 and SGR 1900+14, up to 200 keV. In this case, however, the best-fitting parameters of the NTZ model differ from those found from the fit of *XMM–Newton* data up to 10 keV. In particular, while the temperature of the seed BB is almost unchanged, the value of $\beta_{\rm bulk}$ is always considerably reduced (from 0.3–0.5 to 0.1–0.2) and the twist angle less constrained. This indicates that in the broad-band fit most of the hardening is accounted for by the additional PL component that, in the case of 1E 1841−045 and SGR 1900+14, starts to dominate the spectrum at energies as low as ∼3–4 keV. Of course, this kind of spectral decomposition is certainly possible and may mimic a scenario in which the hard X-ray and soft X-ray emissions are due to two separate processes: for instance soft γ-rays may be produced in a twisted magnetosphere by thermal bremsstrahlung emission from the surface region heated by returning currents or synchrotron emission from pairs created higher up (∼100 km) in the magnetosphere (Thompson & Belobodorov 2005).

In principle, however, spectra produced by resonant cyclotron upscattering of soft photons are expected to develop PL tails that extend up to much higher energies (Baring & Harding 2007; Nobili et al. 2008a). Therefore, it is well possible that our model can consistently explain the whole SED in the 1–200 keV range. If this is the case, the slope of the hard PL tail would be mainly dictated by the properties of the magnetospheric electrons responsible for the upscattering, i.e. their density and velocity distribution. Observationally, the hard X-ray properties of AXPs and SGRs are quite different: while in the range of 4–200 keV the spectra of SGRs are dominated by the non-thermal component and, in the canonical model, well reproduced by a single unbroken PL, AXPs show a sort of turn over and have a non-thermal tail which is initially softer, up to ∼5–8 keV, and then flattens at higher energies. In this picture, 1E 1841−045 seems an exception: its non-thermal emission is well reproduced by a single PL and is therefore more SGR-like (see Rea et al. 2008, and references therein). These properties suggest that, within the resonant Compton scattering scenario, the AXPs spectra require different electron populations. On the other hand, a single electron distribution, as for instance the one we used in the 3D computations presented here, may account for the broad-band emission of SGRs or SGR-like sources.

In order to test this possibility, we cannot use directly our XSPEC table of models, since it has been computed assuming that magnetic scattering is conservative in the electron frame and, for self-consistency, spectra were truncated at 15 keV (see Section 2 for a discussion). Instead, we recomputed the model that best fits the 1–10 keV spectrum of SGR 1900+14 (which parameters are reported in Table 1), this time by extending the computation to the whole 1–200 keV energy range and using a fully relativistic version of the

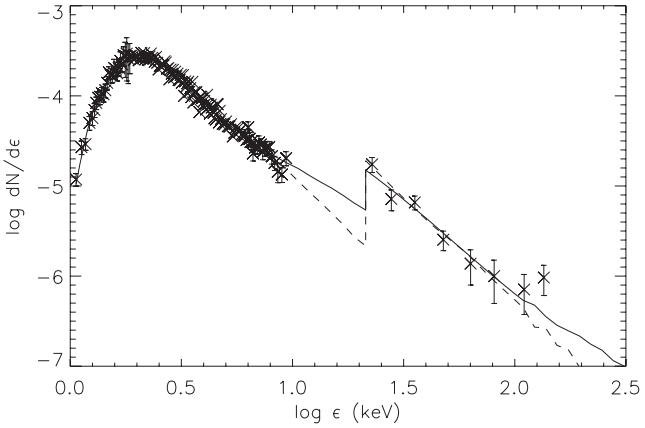

Figure 7. Combined *XMM–Newton* and *INTEGRAL* spectrum of SGR 1900+14. The dashed line is the NTZ spectrum computed for the same values of parameters that best fit the *XMM–Newton* data only (see Table 1), but using the QED cross-sections in the Monte Carlo code. This spectrum is than used to fit the *INTEGRAL* data alone by leaving free only the value of the normalization. This gives $\chi^2 = 1.14$ for 7 d.o.f. and the ratio between the *INTEGRAL* and the *XMM–Newton* normalizations is 8.8. Solid line: same as before but with $\beta_{\rm bulk} = 0.61$, $kT = 0.57$ keV and $\Delta\phi = 0.54$; all parameters are at 3σ from their best-fitting values of the *XMM–Newton* spectrum. Here, the reduced $\chi^2 = 1.07$ for 7 d.o.f. and the ratio between the *INTEGRAL* and the *XMM–Newton* normalizations is 2.8.

Monte Carlo code which incorporates the complete QED scattering cross-section (Nobili et al. 2008b). We also repeated the computation by using slightly different sets of parameters, all within 3σ from their best-fitting values (errors at 1σ are reported in Table 1). As expected, these new spectra differ from those computed in the Thomson limit only at very high energies (>100 keV). Finally, we added to each curve a free normalization constant in the *INTEGRAL* range, to account for intercalibration uncertainties between the two satellites. We then fitted the *INTEGRAL* data by leaving only the intercalibration constant as a free parameter. Results are reported in Fig. 7, where the two curves correspond to: (i) the best-fitting parameters reported in Table 1 and (ii) to a different model in which $\beta_{\rm bulk}$, kT and $\Delta\phi$ have been increased up to their upper limits within the 3σ confidence range from the *XMM–Newton* fit. We found that in both the cases the fit to *INTEGRAL* data is excellent (reduced $\chi^2 = 1.14$ and 1.07, respectively, for 7 degrees of freedom), but the two model normalizations, in the *XMM–Newton* and *INTEGRAL* ranges, differ by a factor of 8.8 and 2.8, respectively, too large to be attributed to intercalibrations uncertainties. Not surprisingly, similar large factors are also found when trying to fit the *XMM–Newton* and *INTEGRAL* data in the range of 6–200 keV with a simple PL model. On the other hand, this simple test proves that the spectral slope of our model in the 20–200 keV range is the same as that of the *INTEGRAL* data. Similar considerations hold in the case of 1E 1841−045. Although a conclusive answer requires a direct fitting of the combined *XMM–Newton* and *INTEGRAL* data with a self-consistent Compton model, which is beyond the scope of this paper, we regard this preliminary finding as promising.

4.4 Caveats and future developments

We caveat that the models presented here are based on a number of simplifying assumptions. First, they are based on a globally twisted dipole model, that only gives an idealized representation of the magnetic field topology. There are now both theoretical

(Beloborodov 2009) and observational [a certain degree of hysteresis in the long-term evolution of SGR 1806−20, Woods et al. (2007); the long-term evolution of the thermal component of the transient AXP XTE J1810−197, Perna & Gotthelf 2008; Bernardini et al. 2008] motivations in favour of a picture in which the twist affects only a limited portion of the magnetosphere, typically the polar region. Furthermore, phase resolved spectroscopy of the two AXPs 1RXS J1708−4009 and 4U 0142+61 in the *INTEGRAL* energy range (Den Hartog et al. 2008a; Den Hartog, Kuiper & Hermsen 2008b) shows dramatic spectral changes with the spin phase. It has been recently suggested that a resonant scattering model in which the magnetic field is locally twisted may catch the essential features of this behaviour (Pavan et al. 2009).

A further point is the nature and velocity distribution of the magnetospheric charges. The NTZ model assumes the presence of mildly relativistic electrons, moving at constant velocity (which is a model parameter) along the closed field lines. Currents flowing in the magnetosphere of a magnetar have been investigated by Beloborodov & Thompson (2007), who concluded that the magnetosphere is populated by pairs with a Lorentz factor of $\gamma \approx 1000$. However, more recent calculations (Nobili, Turolla & Zane, in preparation) show that in the region where $B \gtrsim 2B_Q$ Compton losses efficiently slow down electrons, limiting pair creation to a small region close to the star surface, and allowing for the presence of mildly relativistic particles along much of the circuit.

Finally, angle of view effects have not been accounted for: the emerging spectrum is simply computed by integrating over the whole sky at infinity. This corresponds to the case in which the star is an aligned rotator, i.e. the spin and magnetic axes coincide. As discussed in Nobili et al. (2008a), in order to treat the more general case in which the spin and magnetic axes are not aligned, we also produced a second XSPEC *atable* model by introducing two angles, χ and ξ, which give, respectively, the inclination of the LOS and dipole axis with respect to the star spin axis. This allows us to take into account for the star rotation and hence derive pulse shapes and phase-resolved spectroscopy. The spectral model, *ntzang.mod*, has six free parameters ($\beta_{\rm bulk}, \Delta\phi, \log kT$, χ, ξ plus a normalization constant), that is two more than the one used here. Given that the NTZ model produces a very good fit for the phase-averaged spectra, the inclusion of two further parameters (i.e. the two angles) is not statistically required, as we tested, and will leave χ and ξ unconstrained. On the other hand, having the possibility to infer the viewing geometry may be useful when fitting different outburst states in transient AXPs or when combining information that can be obtained by fitting simultaneously phase-resolved spectra or independently from the study of the pulse profile. Further work in this direction is under way and will be presented in separate papers.

5 CONCLUSIONS

By considering a large sample of magnetars, we found that resonant Compton upscattering by a population of mildly relativistic electrons ($\beta_{\rm bulk} \sim 0.1$–$0.7$) can reproduce the pulse averaged spectra in the range 1–10 keV. At variance with the 1D RCS model adopted in Rea et al. (2008), the approach used in the present investigation consistently accounts for the bulk motion of magnetospheric electrons which results in a more efficient Comptonization of seed thermal photons. This has two main consequences: (i) the required values of the optical depth are lower that those found using the 1D RCS and (ii) NTZ spectra, being intrinsically harder, successfully reproduce also the SGRs PL tail below 10 keV. We found a significant correlation between the 1–10 keV source luminosity and both $\beta_{\rm bulk}$ and kT. This is indeed expected in the RCS model and further supports this scenario to explain the high energy emission from magnetars. Moreover, when restricting to AXPs only, we find hints for a negative correlation between the pulsed fraction and the emitting area. If confirmed, this suggests the presence of a strong thermal gradient on the star surface, which may also be responsible for the slightly different spectrum of 4U 0142+614 and 1E 2259+586, the only two sources for which we could not find a satisfactory fit. Anisotropic surface thermal distributions may arise in the presence of large crustal magnetic fields, as expected in magnetars, because heat is preferentially transferred along the field, resulting in small and confined hot caps (e.g. Geppert, Kueker & Page 2006; Pons, Miralles & Geppert 2009). Moreover, the magnetar surface is also expected to be further heated during bursting activity or by returning currents; in both cases the heat deposition can be substantially anisotropic.

Finally, our conclusions regarding the modelling of the whole SED distribution up to ∼200 keV are still compatible with various scenarios. In the case of 1E 1841−045, 1RXS J1708−4009 and SGR 1900+14, a double component NTZ+PL model fits the combined *XMM–Newton* and *INTEGRAL* data, but it requires a NTZ spectrum quite soft and most of the emission dominated by the additional PL. This is compatible with a scenario in which soft X-ray and hard X-ray emission are ascribed to independent components. On the other hand, there is also the possibility that models of resonant upscattering can successfully describe the whole SED including the hard X-ray tail (eventually by invoking more than one electron population for sources with a spectral turnover at high energies). A conclusive answer requires a direct fitting of the combined *XMM–Newton* and *INTEGRAL* data, with all parameters left free and a new XSPEC table of models computed by using the QED cross-sections. Further work on these topics is in preparation.

ACKNOWLEDGMENTS

SZ acknowledges STFC for support through an Advanced Fellowship. NR is supported by an NWO Veni Fellowship. RT and LN are partially supported by INAF-ASI through grant AAE-I/088/06/0. We thank D. Götz for providing the *INTEGRAL* spectra used in this paper, A. Tiengo and P. Esposito for the data of CXOU J0100-7211 and SGR 1627−41, F. Bernardini and G.L. Israel for the additional 1E 1547.0−5408 data shown in Fig. 6.

REFERENCES

Anders E., Grevesse N., 1989, Geochim. Cosmochim. Acta, 53, 197
Baring M. G., Harding A. K., 2007, Ap&SS, 308, 109
Beloborodov A. M., 2009, ApJ, submitted (arXiv:0812.4873)
Beloborodov A. M., Thompson C., 2007, ApJ, 657, 967
Bernardini F. et al., 2009, A&A, 498, 195
Campana S., Rea N., Israel G. L., Turolla R., Zane S., 2007, A&A, 63, 1047
Den Hartog P. R., Kuiper L., Hermsen W., Kaspi V. M., Dib R., Knödlseder J., Gavriil F. P., 2008a, A&A, 489, 245
Den Hartog P. R., Kuiper L., Hermsen W., 2008b, A&A, 489, 263
Duncan R., Thompson C., 1992, ApJ, 392, L9
Durant M., van Kerkwijk M. H., 2006, ApJ, 650, 1082
Esposito P. et al., 2009, ApJ, 690, L105
Fernandez R., Thompson C., 2007, ApJ, 660, 615
Geppert U., Küker M., Page D., 2006, A&A, 457, 937
Güver T., Özel F., Gögüš E., Kouveliotou C., 2007, ApJ, 667, L73
Haberl F., Freyberg M. J., Briel U. G., Dennerl K., Zavlin V. E., 2004, SPIE, 5165, 104
Hurley K. et al., 2005, Nat, 434, 1098

Lyutikov M., Gavriil F. P., 2006, MNRAS, 368, 690
Lodders K., 2003, ApJ, 591, 1220
Mereghetti S. et al., 2005, ApJ, 628, 938
Mereghetti S., 2008, A&A Rev., 15, 225
Nobili L., Turolla R., Zane S., 2008a, MNRAS, 386, 1527
Nobili L., Turolla R., Zane S., 2008b, MNRAS, 389, 989
Palmer D. M. et al., 2005, Nat, 434, 1107
Pavan L., Turolla R., Zane S., Nobili L., 2009, MNRAS, 395, 753
Perna R., Gotthelf E. V., 2008, ApJ, 681, 522
Pons J., Miralles J. A., Geppert U., 2009, A&A, 496, 207
Rea N., Oosterbroek T., Zane S., Turolla R., Méndez M., Israel G. L., Stella L., Haberl F., 2005, MNRAS, 361, 710
Rea N., Zane S., Lyutikov M., Turolla R., 2007a, Ap&SS, 308, 61
Rea N., Turolla R., Zane S., Tramacere A., Stella L., Israel G. L., Campana R., 2007b, ApJ 661, L65
Rea N. et al., 2007c, MNRAS, 381, 293
Rea N., Zane S., Turolla R., Lyutikov M., Götz D., 2008, ApJ, 686, 1245
Thompson C., Duncan R. C., 1993, ApJ, 408, 194
Thompson C., Beloborodov A. M., 2005, ApJ 634, 565
Thompson C., Lyutikov M., Kulkarni S. R., 2002, ApJ, 274, 332 (TLK)
Tiengo A., Esposito P., Mereghetti S., 2008, ApJ, 680, L133
Woods P. M., Thompson C., 2006, in Lewin W. H. G., van der Klis M., eds, Compact Stellar X-ray Sources. Cambridge Univ. Press, p. 547
Woods P. M. et al., 2004, ApJ, 605, 378
Woods P. M., Kouveliotou C., Finger M. H., Göü E., Wilson C. A., Patel S. K., Hurley K., Swank J. H., 2007, ApJ, 654, 470

This paper has been typeset from a TEX/LATEX file prepared by the author.